Deglaciation of coastal southwestern Spitsbergen dated with *in situ* cosmogenic ^{10}Be and ^{14}C measurements

Nicolás E. Young[1*], Jennifer Lamp[1], Toby Koffman[1], Jason P. Briner[2], Joerg Schaefer[1], Endre F. Gjermundsen[3,4], Henriette Linge[5], Susan Zimmerman[6], Thomas P. Guilderson[6], Derek Fabel[7], Anne Hormes[3,8]

[1]*Lamont-Doherty Earth Observatory, Columbia University, Palisades NY, USA*
[2]*Department of Geology, University at Buffalo, Buffalo NY, USA*
[3]*The University Centre of Svalbard, Longyearbyen, Norway*
[4]*Department of Business and IT, University College of Southeast Norway, Bø, Norway*
[5]*University of Bergen, Bergen, Norway*
[6]*Lawrence Livermore National Laboratory, Center for Accelerator Mass Spectrometry, Livermore CA, USA*
[7]*Scottish Universities Environmental Research Centre, East Kilbride, UK*
[8]*Department of Earth Sciences, University of Gothenburg, Gothenburg, Sweden*

*Corresponding author: Nicolás E. Young
Email: nicolasy@ldeo.columbia.edu; 845.365.8653
Keywords: Quaternary; ice sheets; Svalbard; cosmogenic nuclides, *in situ* ^{14}C,

Abstract

The Svalbard-Barents ice sheet was predominantly a marine-based ice sheet and reconstructing the timing and rate of its decay during the last deglaciation informs predictions of future decay of marine-based ice sheets (e.g. West Antarctica). Records of ice-sheet change are now routinely built with cosmogenic surface exposure ages, but in some regions, this method is complicated by the presence of isotopic inheritance yielding artificially old and erroneous exposure ages. We present forty-six ^{10}Be ages from bedrock (n = 42) and erratic boulders (n = 4) in southwestern Spitsbergen that, when paired with *in situ* ^{14}C measurements (n = 5), constrain the timing of coastal deglaciation following the last glacial maximum. ^{10}Be and *in situ* ^{14}C measurements from bedrock along a ~400 m elevation transect reveal inheritance-skewed ^{10}Be ages, whereas *in situ* ^{14}C measurements constrain 400 m of ice-sheet thinning and coastal deglaciation at 17.4 ± 1.5 ka. Our *in situ* ^{14}C-dated transect, combined with three additional ^{10}Be-dated coastal sites, show that the southwestern margin of the Svalbard-Barents ice sheet retreated out of Norwegian Sea between ~18-16 ka. *In situ* ^{14}C measurements provide key chronological information on ice-sheet response to the last termination in cases where measurements of long-lived nuclides are compromised by isotopic inheritance.

1. Introduction

Geological records that constrain the timing and magnitude of ice-sheet demise during the last deglaciation provide important insights into the response of ice sheets to a warming climate. At its maximum extent during the last glacial cycle the Svalbard-Barents ice sheet (SBIS) was part of the broader Eurasian ice sheet complex with a sea-level equivalent of ~24 m (Hughes et al., 2016). Resting at the northwestern limit of the SBIS, the Svalbard archipelago is one of the few terrestrial locations within the primarily marine-based SBIS footprint. Accordingly, much of our current understanding of how the SBIS evolved through the last glacial cycle is based on archives of ice-sheet change present on Svalbard (Fig. 1; Landvik et al., 1998; Ingólfsson and Landvik, 2013; Hormes et al., 2013; Landvik et al., 2014; Eccleshall et al., 2016). Gauging how the SBIS decayed at the end of the last glaciation can help identify mechanisms of global climate change and inform ice sheet models used to explore the sensitivity of marine-based ice sheets to various climatic and glaciological parameters (Stokes et al., 2015; Patton et al., 2016).

Cosmogenic nuclide measurements are often used to develop detailed chronologies of ice sheet and glacier change (e.g. Balco, 2011; Granger et al., 2013; Ivy-Ochs and Briner, 2014). On Svalbard, there have been a number of efforts to reconstruct SBIS behavior during the last glacial cycle using cosmogenic nuclides with mixed success. One limitation is that much of Svalbard does not host the quartz-bearing rocks required for ^{10}Be measurements, and accordingly the geographic scope of cosmogenic nuclide-based measurements is relatively restricted. Nonetheless, the first ^{10}Be ages from Svalbard were used to propose that ice-free regions in northwestern Svalbard existed during last glacial maximum (Landvik et al., 2003). However, while ^{10}Be ages older than ~75 ka defined the maximum SBIS thickness in NW Svalbard, these old ^{10}Be ages do not preclude the presence of widespread and systematic isotopic inheritance on the landscape. Using the same approach, a number of ^{10}Be ages from western Svalbard and Nordaustlandet help constrain the dimensions of the SBIS during the last glacial cycle (Hormes et al., 2011; 2013; Landvik et al. 2013; Gjermundsen et al., 2013; Fig 1). Most recently, ^{10}Be and ^{26}Al measurements from high-elevation bedrock suggest that Svalbard's alpine landscape has survived repeated glaciations through the Quaternary suggestive of a minimally erosive ice sheet (Gjermundsen et al., 2015). Although these studies place broad constraints on SBIS behavior through the last glacial cycle and longer, they also suffer from somewhat geographically and chronologically scattered ^{10}Be ages, making it difficult to develop detailed millennial-scale chronologies of ice-sheet change. Collectively, these studies highlight a landscape that is challenging for developing cosmogenic-nuclide based chronologies of ice-sheet change, likely due to the widespread presence of non-erosive cold-based ice and its variable imprint on the landscape (Landvik et al., 2014).

Surface exposure dating in glacial landscapes relies on the assumption that cosmogenic nuclides that accumulated on the landscape prior to the most recent episode of exposure have been removed by ~2-3 m of subglacial erosion during the latest interval of ice cover. In settings dominated by warm-based and erosive ice, this assumption is typically valid, but at high-latitude locations, minimally erosive polythermal and cold-based ice can result in cosmogenic nuclide datasets that are influenced by isotopic inheritance (e.g. Håkansson et al., 2008; Corbett et al., 2013; Balco et al., 2014; Young et al., 2016). Isotopic inheritance occurs when ice is unable to erode through the ~2-3 m of rock required to reset the cosmogenic clock between periods of surface exposure and the resulting nuclide concentration is an aggregate of 2 or more distinct periods of exposure. Inheritance is also possible within landscapes where despite 2-3 m of erosion during the latest interval of glaciation, deep subsurface nuclide accumulation in periods of prolonged surface exposure between glaciations, results in excess nuclide inventories that pre-date the most recent period of ice cover (Briner et al., 2016).

Whereas long-lived or stable nuclides such as ^{10}Be ($t_{1/2}$ = 1.387 Ma; Chmeleff et al., 2010) must be removed from the landscape via sufficient subglacial erosion, *in situ* ^{14}C is unique because its relatively short half-life ($t_{1/2}$ = 5730 years) allows for previously accumulated *in situ* ^{14}C to decay away to undetectable levels after ~30 ka of simple burial of a surface by ice without the aid of subglacial erosion. *In situ* ^{14}C measurements are perhaps most powerful when paired with ^{10}Be to resolve complex exposure-burial histories (e.g. Goehring et al., 2011), but *in situ* ^{14}C measurements are also particularly attractive in environments characterized by minimally erosive ice that is not capable of resetting the cosmogenic clock between periods of exposure. Measuring several nuclides in conjunction yields a more complete quantitative understanding of ice-sheet fluctuations over multiple time-scales, but *in situ* ^{14}C measurements are perhaps best suited to constrain the timing of the last deglaciation in settings where long-lived nuclides such as ^{10}Be run a much higher risk of carrying inheritance from prior exposure (e.g. Briner et al., 2014; Johnson et al., 2017). Despite its potential, *in situ* ^{14}C is rarely utilized because of the difficulty of extracting ^{14}C from the mineral quartz in geological samples (e.g. Lifton et al., 2001; Balco et al., 2016).

We present 46 ^{10}Be ages, 5 *in situ* ^{14}C ages and 5 ^{26}Al ages from 4 sites in southwestern Spitsbergen to constrain the timing of coastal deglaciation following the last glacial maximum. A component of our ^{10}Be ages are influenced by isotopic inheritance, but our population of ^{10}Be ages is sufficiently large to constrain the timing of coastal deglaciation in southwestern Spitsbergen. Combined *in situ* ^{10}Be, ^{14}C, and ^{26}Al in 5 bedrock samples along a ~400 m elevation transect reveal that ^{10}Be and ^{26}Al concentrations yield an ambiguous timing of deglaciation and a complex long-term exposure history but corresponding *in situ* ^{14}C measurements robustly constrain millennial-scale ice-sheet thinning.

2. Setting and Methods

Our study area is Hornsund (76.97°N, 15.70°E), located in southwestern Spitsbergen (Fig. 1 and Fig. 2). Several independent glaciers feed into the primary Hornsund channel (Fig. 1 and Fig. 2) and, at present, ~800 km^2 of Hornsund's ~1200-km^2 drainage basin is glaciated with glacier retreat during the observational record averaging ~70 m/a (Blaszczyk et al., 2013). At the head of Hornsund, a tidewater glacier is currently located ~13 km east of its late Holocene maximum extent, which is marked by a prominent moraine that was emplaced at Treskelen just before 1.9 $\pm$ 0.3 ka based on recent ^{10}Be ages (n= 4; Philipps et al., 2017). During the last glacial cycle, Hornsund hosted a SBIS outlet glacier that was part of the western margin of the SBIS. The western SBIS is thought to have advanced out to the continental shelf 3 times during the last glacial cycle during Marine Isotope Stage (MIS) 5d, MIS 5b, and MIS 2 with retreat from the outer shelf underway as early as ~23-20 ka (Mangerud et al., 1998; Jessen et al., 2010; Hormes et al., 2013; Eccleshall et al., 2016). A single minimum limiting radiocarbon age from near Hornsund indicates that by ~12.1 cal ka BP ice was less extensive than it is today (Birkenmajer and Olsson, 1998; Hormes et al., 2013). The long-term pattern of SBIS advance and retreat in western Svalbard is largely based on the Kapp Ekholm sediment section located at the inner reaches of Isfjorden, which displays alternating units of glacial till and marine sediments (Fig. 1). Because Kapp Ekholm is situated only ~14 km from modern ice, the marine sediment units likely mark intervals when Svalbard glaciers were likely not much larger than today (Mangerud et al., 1998; Eccleshall et al., 2016).

We collected 46 samples for ^{10}Be dating, 5 samples for ^{26}Al measurement and 5 samples for *in situ* ^{14}C measurements along the southwestern coast of Spitsbergen. Thirty-four ^{10}Be samples are from the Hornsund region and are divided into 4 distinct groups (Fig. 1 and Fig. 2): 1) a series of nunatak and bedrock ridges (n = 18), 2) an elevation transect at Torbjørnsenfjellet on the north side of Hornsund (n = 5; Fig 3A), 3) an elevation transect at Wurmbrandegga on the south side of Hornsund (n = 7; Fig. 3B), and 4) boulders perched on a bedrock ridge adjacent to, but beyond, the late Holocene ice extent at Treskelen (n = 4). We measured *in situ* ^{14}C and ^{26}Al in each bedrock sample from the Torbjørnsenfjellet elevation transect. We also collected 4 bedrock samples from surfaces immediately outboard of the late Holocene terminal moraine (<150 m) at Scottbreen (77.54°N, 14.36°E) located ~70 km northwest of Hornsund (Fig. 1). Lastly, we collected 4 ridgeline bedrock samples from Fløyfjellet (77.41°N, 14.09°E) located ~60 km northwest of Hornsund and 4 bedrock samples from summits near Torellbreen (77.31°N, 14.09°E) located between Fløyfjellet and Hornsund (Fig. 1).

Samples were collected in 2013 and 2014 with a hammer and chisel, and a Trimble GeoXT and Tempest antenna GPS receiver with a vertical uncertainty of ±0.5 m was used to record sample location and elevation. A handheld clinometer was used to measure topographic shielding by the surrounding topography. Beryllium-10 samples were processed at the Buffalo Cosmogenic Laboratory (n = 29), Lamont-Doherty Earth Observatory (LDEO) Cosmogenic Nuclide Laboratory (n = 13; n = 5 ^{26}Al samples), and the Scottish Universities Environmental Research Centre (SUERC; n = 4) following standard extraction methods for ^{10}Be and ^{26}Al (Schaefer et al., 2009). *In situ* ^{14}C samples were processed at LDEO and measured ^{14}C concentrations are blank-corrected using a long-term laboratory blank. (Goehring et al., 2014; see Table 2 and Table 3). Accelerator mass spectrometric measurements for LDEO and Buffalo samples were made at Lawrence Livermore National Laboratory – Center for Accelerator Mass Spectrometry, and the remaining samples were measured at SUERC (Table 1). Surface exposure ages were calculated using the Arctic (^{10}Be and ^{26}Al) and western Greenland (^{14}C) production rate calibration datasets (Young et al., 2013; 2014) and ‘Lm’ scaling (Lal, 1991; Stone, 2000) since the effects of changes in the geomagnetic field are minimal at this high latitude. Ages are calculated using version 3 of the CRONUS calculator code that implements an updated treatment of muon-based nuclide production (Balco et al., 2008; Balco, 2017). We do not correct nuclide concentrations for snow-cover or erosion; samples are primarily from windswept locations and many sampled surfaces displayed primary glacial features. In addition, we make no correction for isostatic rebound because the effects of uplift on nuclide production are likely offset atmospheric compression, albeit these effects are difficult to quantify (Staiger et al., 2007). Individual exposure ages are presented and discussed with 1-sigma analytical uncertainties, and when comparing our results to independently dated records of ice sheet or environmental change, the production rate uncertainty is propagated through in quadrature.

3. Results

Four individual ^{10}Be ages at Scottbreen are 18.8 ± 0.5, 17.9 ± 0.3, 16.3 ± 0.3 and 17.8 ± 0.4 ka (all bedrock). At Fløyfjellet, four individual ^{10}Be ages are 16.2 ± 0.4, 16.2 ± 0.4, 15.9 ± 0.4 and 15.3 ± 0.4 ka (all bedrock), and at Torellbreen, four additional ^{10}Be ages are 23.0 ± 0.5, 17.3 ± 0.5, 16.0 ± 0.3 and 14.3 ± 0.3 ka (all bedrock). At Hornsund, the coastal nunatak and ridgeline ^{10}Be ages span 5.6 ± 0.1 to 36.5 ka ± 0.7 ka (n = 18; bedrock). The Wurmbrandegga elevation transect has ^{10}Be ages ranging between 10.9 ± 0.3 ka to 13.8 ± 0.3 ka (n = 7; bedrock), and the Torbjørnsenfjellet elevation transect has ^{10}Be ages ranging from 16.0 ± 0.3 ka to 36.3 ± 0.6 ka (n=5; bedrock). The up-fjord ^{10}Be ages from erratic boulders perched on bedrock range from 12.6 ± 0.4 to 15.4 ka ± 0.9 ka (n=4). Lastly, ^{26}Al and *in situ* ^{14}C ages at Torbjørnsenfjellet range from 17.2 ± 1.1 ka to 35.8 ± 1.8 ka and 16.7 ± 2.9 ka to 18.5 ± 2.7 ka, respectively (Tables 1 - 3). Measured $^{26}Al/^{10}Be$ ratios range from 7.38 ± 0.64 to 5.77 ± 0.38.

4. Multiple nuclides constrain the timing of deglaciation and erosion regimes

Scottbreen, Fløyfjellet and Torellbreen

The mean of four ^{10}Be ages at Scottbreen is 17.7 ± 1.2 ka (production rate uncertainty included) and it is tempting to use this age constraint as the timing of local coastal deglaciation. However, these four samples are all from bedrock that are in close proximity to one another (~300 m distance and 38 m elevation) and are located immediately outside Scottbreen's historical maximum extent. Landscapes positioned near glacial maxima that spend a large proportion of a glacial cycle ice free may be affected by small, uniform amounts of isotopic inheritance that yield consistent, but slightly too old ^{10}Be ages (Briner et al., 2016). Because the Scottbreen samples are from such close proximity to each other, it is possible these ^{10}Be bedrock ages simply constrain a local ^{10}Be inventory that contains a small, and uniform, amount of isotopic inheritance. In addition, the age 17.7 ± 1.2 ka would indicate that Scottbreen retreated within its late Holocene maximum extent rather early following the last glacial maximum. Nonetheless, while small amounts of inheritance may be influencing our Scottbreen ^{10}Be ages, we tentatively use 17.7 ± 1.2 ka as the timing of local deglaciation. At Fløyfjellet, all ^{10}Be ages overlap at 1-sigma indicating that deglaciation occurred at 15.9 ± 0.7 ka. The four ^{10}Be ages at Torellbreen are more scattered (Table 1), but the individual ^{10}Be ages of 14.3 ± 0.3 ka, 16.0 ± 0.3 ka, and 17.3 ± 0.5 ka (mean = 15.9 ± 1.6 ka) are consistent with the timing of deglaciation at Fløyfjellet and Scottbreen. Combined, ^{10}Be ages indicate that deglaciation at Scottbreen, Fløyfjellet, and Torellbreen occurred at 17.7 ± 1.2 ka, 15.9 ± 0.7 ka, and 15.9 ± 1.5 ka (Fig. 1).

The consistency between the timing of deglaciation at Scottbreen (17.7 ± 1.2 ka), Fløyfjellet (15.9 ± 0.7 ka) and Torellbreen (15.9 ± 1.5 ka), which all post-date the last glacial maximum, is suggestive of ^{10}Be ages that are accurately recording the timing of deglaciation and are not influenced by inheritance. Moreover, ^{10}Be ages at all three locations are solely from bedrock suggesting that a warm-based SBIS was able to erode through the ~2 m of rock required to reset the cosmogenic clock along Spitsbergen's southwestern coast. Ultimately, we cannot rule out that our ^{10}Be measurements from Scottbreen, Fløyfjellet and Torellbreen are systematically influenced by deep subsurface nuclide accumulation during periods of prolonged surface exposure and contain a small amount of isotopic inheritance (Briner et al., 2016). However, similar ^{10}Be ages that are influenced by systematic deep subsurface nuclide accumulation would likely require near-identical exposure histories and total erosion depths during periods of ice cover across all three sites. We prefer the more likely scenario where the consistency in ^{10}Be ages at Scottbreen, Fløyfjellet, and Torellbreen simply reflect the similar timing of deglaciation across these sites and the erosional efficiency of a warm-based SBIS (Fig. 1).

Hornsund

Constraining the timing of initial deglaciation at Hornsund is more challenging. Here, we consider ^{10}Be ages within the context of their morphostratigraphic position. A series of ages from coastal nunataks and ridges range from 5.6 ± 0.1 ka to 36.5 ± 0.7 ka, show no clear trend with elevation as would be expected with glacier thinning, and adjacent samples from similar elevations often have drastically different ages (Fig. 2; black text/white boxes; Table 1). A number of coastal ages are older than 20 ka and there appears to be a mode of ^{10}Be ages centered at ~30-35 ka (Fig. 2). These ages could constrain an initial pulse of ice-sheet thinning or an episode of MIS 3 deglaciation followed by non-erosive MIS 2 burial. However, three ^{10}Be ages of 34.5 ± 0.6 ka, 36.4 ± 0.7 ka and 36.5 ± 0.7 ka are from ~110m asl whereas slightly inland there are ^{10}Be ages of 18.7 ± 0.3 ka and 17.3 ± 0.6 from ~750 and 680 m asl. It is possible that these younger ages inland were affected by post-deglaciation mass wasting events, but our ages of >30 ka that pre-date the last deglaciation rest in a region where subglacial erosion during periods of ice cover was likely not as intense as in the primary Hornsund channel (Fig. 2). The large spread in ^{10}Be ages and a ^{10}Be age-elevation relationship that violates simple morphostratigraphy is likely due to a combination of isotopic inheritance in low-erosion zones, combined with sampling bedrock surfaces where the original post-deglaciation surface has not been preserved. Radiocarbon ages from marine sediments in a variety of settings indicate that the ice sheet extended ~70 km west of Hornsund to the continental shelf edge until ~23 ka (Fig. 1). Moreover, a recent synthesis of Eurasian ice sheet extent suggests that ice in the Barents sector was at its maximum between ~23-20 ka making it unlikely that the Hornsund mouth deglaciated at or prior to ~23-21 ka as suggested by a number of our ^{10}Be ages older than 23 ka (i.e. 35 ka mode in ^{10}Be ages; Fig. 1 and Fig. 2).

Torbjørnsenfjellet

Beryllium-10 and *in situ* ^{14}C measurements from the Torbjørnsenfjellet elevation transect constrain the timing of initial deglaciation of the Hornsund fjord mouth. In descending elevational order: the highest elevation sample (TORB-1; 633 m asl) has a ^{10}Be age of 16.0 ± 0.3 ka followed by ^{10}Be ages of 18.3 ± 0.3 ka (TORB-2; 515 m), 36.3 ± 0.6 ka (TORB-4; 279 m), 25.8 ± 0.4 ka (TORB-3; 252 m), and 20.1 ± 0.3 ka (TORB-5; 225 m). The oldest ages rest in the middle of the elevation transect and the youngest age is also the highest elevation sample (Fig. 2). This ^{10}Be age-elevation distribution reveals that ^{10}Be ages are not accurately recording the timing of glacier thinning and deglaciation because ^{10}Be ages do not get younger with decreasing elevation nor are they statistically indistinguishable, the latter of which would suggest rapid (within dating resolution) deglaciation of all sample sites. Corresponding *in situ* ^{14}C ages, however, display a much different age-elevation relationship. Paired ^{10}Be and *in situ* ^{14}C ages for TORB-1 and TORB-2, our highest elevation samples, statistically overlap at 1-sigma indicating these samples do not contain inherited ^{10}Be (Fig. 3; Table 1). The mid-transect samples with ^{10}Be ages of 36.3 ± 0.6 ka (TORB-4) and 25.8 ± 0.4 ka (TORB-3), have significantly younger ^{14}C ages of 16.9 ± 3.1 ka and 17.3 ± 3.2 ka indicating that they contain a ^{10}Be inventory equating to 19.4 ± 3.2 ka and 8.5 ± 3.2 ka of excess ^{10}Be that accumulated during a previous period(s) of surface exposure. The lowest elevation sample (TORB-5) has a ^{10}Be age of 20.1 ± 0.3 ka and a ^{14}C age 16.7 ± 2.9 ka. We note that the 1-sigma analytical uncertainties of our *in situ* ^{14}C measurements range from 4-7%, but that these measurements equate to exposure ages with uncertainties that range from ~15-23%. Exposure age uncertainties range from ~15-23% because our measured concentrations intersect the ^{14}C production-time curve where small changes in ^{14}C concentration equate to large changes in exposure age as one approaches surface saturation (nuclide production = decay; Table 2). Regardless, our *in situ* ^{14}C measurements are able to quantify inherited ^{10}Be in 3 of our 5 transect samples and, moreover, *in situ* ^{14}C ages are statistically indistinguishable and average 17.4 ± 0.7 ka (n = 5; Fig. 2; Fig.3; Table 2). When accounting for the uncertainty in the production-rate calibration dataset (7.5%; Young et al, 2014), our ^{14}C measurements reveal glacier thinning across our sample sites at the Hornsund mouth at 17.4 ± 1.5 ka.

Whereas paired ^{10}Be–^{14}C measurements at Torbjørnsenfjellet constrain the amount of isotopic inheritance and timing of deglaciation to 17.4 ± 1.5 ka, paired ^{26}Al – ^{10}Be measurements offer a long-term perspective of surface exposure and burial of the Torbjørnsenfjellet ridgeline. TORB-1 and TORB-2, which have statistically identical ^{10}Be and *in situ* ^{14}C ages, have ^{26}Al/^{10}Be ratios consistent with constant exposure (Fig. 4; Table 1). Our mid-transect samples (TORB-4 and TORB-3) contain inherited ^{10}Be and measured ^{26}Al/^{10}Be ratios suggest some degree of prolonged burial (Fig. 4). Although the TORB-5 ^{10}Be and *in situ* ^{14}C ages overlap at 2-sigma, suggestive of continuous exposure, the corresponding ^{26}Al/^{10}Be ratio of 5.77 ± 0.38 is inconsistent with constant exposure. Because all of the transect *in situ* ^{14}C ages are statistically identical and constrain the most recent period of exposure, we use the average *in situ* ^{14}C age to quantify the exposure-burial history of the Torbjørnsenfjellet samples sites prior to the last ~17.4 ka. Rather, we subtract 17.4 ka worth of exposure from each paired ^{26}Al – ^{10}Be measurement to quantify pre-17.4 ka exposure and burial at each sample location (Fig. 4) This approach results in either completely depleting the ^{10}Be inventory (TORB-1) or a corrected ^{26}Al/^{10}Be ratio that overlaps zero (TORB-2), both further suggestive of one period of constant exposure for these sites. At TORB-5, our approach results in subtracting more ^{26}Al than what was measured, but points to the presence of a small amount of excess ^{10}Be, equating to 3.4 ± 2.9 kyr of exposure. The corrected ratios for our mid-transect samples reveal a significant amount of pre-17.4 ka surface burial equating to ~54 – 570 kyr, albeit with large uncertainties (Fig. 4).

Wurmbrandegga and Treskelen

At the Wurmbrandegga elevation transect, which is located ~12 km up-fjord from Torbjørnsenfjellet and therefore must have deglaciated at or after 17.4 ± 1.5 ka, six of seven ^{10}Be ages are indistinguishable and indicate that this portion of Hornsund deglaciated at 13.3 ± 0.6 ka (Fig. 2; Fig. 3). Unlike the Torbjørnsenfjellet transect, we find no evidence that the samples at Wurmbrandegga contain inherited ^{10}Be, which is suggestive of a greater total erosion depth than the Torbjørnsenfjellet site during periods of ice cover. Finally, our eastern-most ^{10}Be ages from perched boulders positioned ~13 km up-fjord from Wurmbrandegga at Treskelen indicate that final deglaciation of the fjord occurred by 13.0 ± 0.7 ka (n = 3) after removal of an older outlier (15.4 ± 0.9; Fig. 2). Combined, our ^{10}Be and *in situ* ^{14}C ages suggest that the Hornsund mouth deglaciated at 17.4 ± 1.5 ka, with ice remaining near the fjord mouth for several thousand years before complete deglaciation between 13.3 ± 0.6 ka and 13.0 ± 0.7 ka (Fig. 2 and Fig. 5). Alternatively, our ice-margin chronology allows for initial deglaciation of the Hornsund mouth at 17.4 ± 1.5 ka followed by continued fjord deglaciation, an ice-margin re-advance beyond the Wurmbrandegga transect with inner fjord deglaciation between 13.3 ± 0.6 ka and 13.0 ± 0.7 ka. However, we are unaware of any sediment packages within the fjord that are suggestive of a significant re-advance of the Hornsund glacier.

5. The Hornsund outlet glacier during the last glacial cycle

^{10}Be and in situ ^{14}C ages versus traditional radiocarbon constraints

In situ ^{14}C ages indicate that the Hornsund outlet glacier thinned ~400 m at 17.4 ± 1.5 ka, consistent with the timing of coastal deglaciation at Scottbreen (17.7 ± 1.2 ka), Fløyfjellet (15.7 ± 0.7 ka) and Torellbreen (15.9 ± 1.6 ka; Fig. 1). However, previously published records suggest that deglaciation of the western Svalbard coast occurred much later. A series of radiocarbon ages from marine sediments place the SBIS margin out on the shelf edge between ~23-20 ka with deglaciation of the SW Spitsbergen coast constrained to ~13.7-11.7 cal ka BP based on minimum-limiting radiocarbon ages from raised marine sediments (Fig. 1 and Fig. 2; Landvik et al., 1998; Hormes et al., 2014). It is possible that all of our deglaciation ages constrain initial ice-sheet thinning and unroofing of our sampling sites prior to deglaciation of the coastal lowlands. However, with the exception of the Torellbreen site located north of Hornsund, all of our deglaciation ages span relatively low elevations that should capture the timing of coastal deglaciation (Table 1). Alternatively, there is a possible ~5 kyr offset in the timing of Hornsund deglaciation as defined by our *in situ* ^{14}C ages versus the minimum-limiting radiocarbon of 12.1 cal ka BP. And, the deglaciation age provided by the Wurmbrandegga elevation transect located only ~12 km up-fjord from the outer coast is 13.3 $\pm$ 0.6 ka; ~4 ka younger than the Hornsund mouth *in situ* ^{14}C age, but still older than the minimum-limiting 12.1 cal ka BP deglaciation age. One explanation is that the minimum-limiting 12.1 cal ka BP age does not closely constrain the timing of deglaciation and that deglaciation occurred at either 17.4 $\pm$ 1.5 ka or just before 13.3 $\pm$ 0.6 ka. Or, the Hornsund outlet glacier thinned to at least 225 m asl at 17.4 $\pm$ 1.5 ka (lowest sample in elevation transect) but occupied the fjord mouth for another several thousand years before final deglaciation. A final possibility is that our *in situ* ^{14}C measurements contain inherited *in situ* ^{14}C from a previous period of exposure that occurred prior to 13.3 $\pm$ 0.6 ka or 12.1 cal ka BP.

Modeling ^{10}Be and in situ ^{14}C inventories

To assess our measured ^{10}Be and *in situ* ^{14}C inventories at Torbjørnsenfjellet, we use the Svalbard glaciation curve over the last glacial cycle to model the possible ^{10}Be and *in situ* ^{14}C accumulation history at our sample sites. The Svalbard glaciation curve (Fig. 5) suggests a dynamic SBIS advanced onto the continental shelf several times over the last glacial cycle; between these glacial maxima, the SBIS retreated back to an ice configuration similar to today (Mangerud et al., 1998; Eccleshall al., 2016; Fig. 1 and Fig. 5). Notably, the SBIS occupied the shelf or shelf edge during MIS 6, MIS 5d, MIS 5b, MIS 2, with an additional, although likely not as extensive, advance during MIS 4. Although this Svalbard glaciation history is largely based on the Kapp Ekholm section at the head of Isfjorden (Fig. 1), a non-finite radiocarbon age of >40 ka from shell fragments suggests that Hornsund may have deglaciated at least once prior to the most recent episode of deglaciation (Landvik et al., 1998).

This template of SBIS advance and retreat provides a unique opportunity assess the likelihood of our coastal Torbjørnsenfjellet bedrock sites yielding significant inherited ^{10}Be coupled with *in situ* ^{14}C inventories that have minimal or no inheritance. We assume no prior nuclide inventory at our bedrock sites at the termination of MIS 6 (Fig. 5). Next, we allow surface exposure and nuclide accumulation during MIS 5e, 5c, 5a and 3, burial and nuclide decay during MIS 5d, 5b, 4 and 2, and assume a 'true' deglaciation of ~13.3 ka as defined by our nearby Wurmbrandegga ^{10}Be ages. We want to assess the maximum amount of potential inherited nuclides at Torbjørnsenfjellet so we assume no bedrock erosion during periods of ice cover; only nuclide decay via burial decreases the nuclide inventory. When modeling ^{10}Be and *in situ* ^{14}C concentrations using these assumptions, our Torbjørnsenfjellet bedrock sites would have ^{10}Be and *in situ* ^{14}C concentrations equating to exposure ages of ~81 ka and 14.6 ka, respectively (Fig. 5).

Our model suggests that using the Svalbard glaciation curve as a template for surface exposure and burial results in ^{10}Be and *in situ* ^{14}C concentrations similar to what we measured – old ^{10}Be ages coupled with younger *in situ* ^{14}C ages. In addition, our approach results in a small amount of inherited *in situ* ^{14}C at our Torbjørnsenfjellet sample sites. Rather, the modeled duration of MIS 2 burial is not long enough to completely remove the accumulated MIS 5e through MIS 3 inventory of *in situ* ^{14}C (Fig. 5). Because the duration of MIS 2 burial results in a small amount of inherited *in situ* ^{14}C in our model experiment, we next assume that our measured *in situ* ^{14}C concentrations are influenced by inheritance and then calculate the timing of deglaciation needed to result in our measured *in situ* ^{14}C concentrations. With this approach, our measured *in situ* ^{14}C concentrations are achieved if deglaciation occurs at ~15.6 ka, which is suggestive of a 'true' deglaciation age that is ~2 ka younger than our measured *in situ* ^{14}C ages. However, our model set up is tuned to allow for the maximum amount of inherited *in situ* ^{14}C because we assume no glacial erosion during periods of ice cover, which is not supported by our measured ^{10}Be ages, which vary across the transect and imply varying degrees of glacial erosion. The modeled exposure-burial histories result in ^{10}Be concentrations that equate to ~81 - 85 ka, whereas our measured ^{10}Be ages from the Torbjørnsenfjellet transect range from ~16 to ~36 ka (Fig. 3C). This disparity between the modeled and measured ^{10}Be ages suggests that the Torbjørnsenfjellet sample sites either experienced some degree of glacial erosion that has stripped away ^{10}Be (and *in situ* ^{14}C) from the bedrock sites and/or our sample sites experienced less surface exposure during the last glacial cycle than what we modeled using the Svalbard glaciation curve.

The minor differences in our measured versus modeled ^{10}Be and *in situ* ^{14}C inventories is likely due to variable glacial erosion during periods of ice cover and/or uncertainty in the exact duration that our bedrock sites experienced ice-cover and nuclide decay versus the exact duration of ice-free conditions and nuclide accumulation. Despite these differences, our model captures the overall pattern of older ^{10}Be ages influenced by isotopic inheritance coupled with *in situ* ^{14}C ages that are much younger. The maximum inheritance scenario that does not account for glacial erosion results in *in situ* ^{14}C concentrations with only a small degree of inheritance (~2 ka). Glacial erosion during periods of ice cover, as suggested by the spread in ^{10}Be ages, would not only remove a portion of previously accumulated ^{10}Be, but also remove *in situ* ^{14}C resulting in bedrock sample sites that do not contain previously accumulated ^{14}C prior to the most recent period of exposure. Thus, it is unlikely that our *in situ* ^{14}C ages are influenced by inheritance and that the 'true' age of deglaciation at the fjord mouth is 17.4 $\pm$ 1.5 ka (Fig. 1; Fig. 3C).

6. Coastal deglaciation of western Spitsbergen

Our ^{10}Be and *in situ* ^{14}C ages indicate that the region of coastal southwestern Spitsbergen south of Isfjorden deglaciated between ~18-16 ka (Fig. 1). This timing of coastal deglaciation in southwestern Spitsbergen is broadly consistent with the timing of coastal deglaciation in northwestern Spitsbergen, which is constrained to ~17.9 to 15.6 cal ka BP based on the oldest published coastal radiocarbon ages, and low-elevation ^{10}Be ages from the region (Fig. 1; Table 4). Although a number of older ^{10}Be ages from northwestern Spitsbergen range from ~ 25.0 to 19.3 ka (Fig. 1), these ages are mainly from high-elevation nunataks and likely record initial ice sheet thinning rather than coastal deglaciation. Two older ^{10}Be ages of 26.7 $\pm$ 3.9 ka and 28.3 $\pm$ 2.1 ka from erratics in Nordaustlandet may record the timing of early coastal deglaciation considering their low elevations (165 and 123 m asl), but their anomalously old ages could simply represent the presence of cold-based ice and ^{10}Be inheritance as suggested by the original authors (Hormes et al., 2011; Fig. 1; Table 1). It appears that the timing of coastal deglaciation in northwestern and southwestern Spitsbergen (between Hornsund and Scottbreen) is perhaps similar, but deglaciation through Isfjorden trough occurred much later (Fig. 1; Fig. 5). A relatively dense transect of radiocarbon ages extending from the outer shelf to near the modern ice margin in Isfjorden indicates that although the timing of initial retreat from the shelf edge is similar to the timing of initial ice-margin retreat west of Hornsund (~23 ka), ice at Isfjorden remained near the shelf edge until as late as ~17.9 cal ka BP (Fig. 1). In addition, the Isfjorden mouth did not deglaciate until ~14.3 cal ka BP, 1.5-3.5 kyr later than the timing of coastal deglaciation in southwestern Spitsbergen (Fig. 1). A record of ice-rafted detritus (IRD) located immediately southwest of Hornsund reveals peaks in IRD at ~18.7 ka and ~16.3 ka, suggestive of increased calving and ice-margin retreat at these time (Fig. 5). This increase in IRD deposition is broadly correlative with the timing of coastal deglaciation as constrained by our ^{10}Be and *in situ* ^{14}C measurements (~18-16 ka); however, the resolution of our record, and in particular *in situ* ^{14}C-based age of deglaciation (17.4 $\pm$ 1.5 ka), prevent us from linking the timing of deglaciation to any one IRD peak (Fig. 5).

The timing of coastal deglaciation appears to have differed between Isfjorden and southwestern Spitsbergen, but the relatively sparse number of radiocarbon constraints between the outer shelf and coast at Hornsund prevents us from determining if ice in this sector stayed near the shelf edge for several thousand years or gradually retreated between ~23 and 17.4 $\pm$ 1.5 ka (Fig. 1 and Fig. 5). Existing age constraints from Isfjorden and Hornsund allow us to place millennial- to centennial-scale retreat of the ice-margin into a long-term context (Fig. 5). At Hornsund, the SBIS retreated at a millennially averaged rate of ~10 m/a between ~23 and 17.4 ka, and ~3 m/a between 17.4 and 13.3 ka. However, the 17.4 $\pm$ 1.5 ka constraint along the Hornsund transect at Torbjørnsenfjellet requires ~400 m of ice-sheet thinning in addition to constraining the lateral retreat of the ice margin. Following deglaciation at Wurmbrandegga, the ice margin retreated between ~13.3 and 13.0 ka at the rate of ~43 m /a (Fig. 5). At Isfjorden, initial ice-margin retreat occurred at ~3 m/a between 23.2 cal ka BP and 17.9 cal ka BP followed by a slightly faster rate of retreat of ~13 m/a between ~17.9 and 14.5 cal ka BP. Afterwards, retreat rates increased significantly between ~14.5 and 14.3 cal ka BP (~400 m/a), with another pulse of rapid deglaciation centered on ~12.3 cal ka BP (~120 m/a; Fig. 5). We note that these retreat rates should be considered minimum or net retreat rates because our methods are limited in their ability to identify pulses of fast ice retreat and almost certainly smooth over episodes of faster ice retreat.

It appears that initial retreat of the western margin of the SBIS occurred as early as ~23 ka, synchronous with the initial rise in boreal summer insolation at ~24-23 ka and consistent with the onset of initial retreat of the southern margin of the Laurentide ice sheet (e.g. Ullman et al., 2015), but pre-dating any significant rise in eustatic sea level. However, SBIS retreat rates remained relatively slow until at least 17.9 ka and perhaps as late as ~14.5 ka as suggested by the Isfjorden recession chronology. Indeed, whereas initial retreat was contemporaneous with rising summer insolation, elevated retreat rates were not achieved until several millennia later, contemporaneous with rising temperatures as recorded in Greenland ice cores at the onset of the Bølling-Allerød (Fig. 5).

7. Conclusions

Deglaciation of the southwestern Spitsbergen coast likely occurred between ~18 – 16 ka based on new ^{10}Be and *in situ* ^{14}C measurements from four separate sites along ~60 km of southwestern Spitsbergen. ^{10}Be measurements in bedrock along a ~400 m elevation transect display varying amounts of isotopic inheritance and are unable to constrain the timing of deglaciation or ice-sheet thinning, but complimentary *in situ* ^{14}C measurements are statistically identical and mark an episode of ice-sheet thinning at 17.4 $\pm$ 1.5 ka. Following coastal deglaciation, the middle of Hornsund deglaciated by 13.3 $\pm$ 0.6 ka with complete fjord deglaciation by 13.0 $\pm$ 0.7 ka. Our dataset indicates that the timing of coastal deglaciation in southwestern Spitsbergen was significantly earlier than previous estimates based on a limited number of minimum-constraining radiocarbon ages. Previously published age constraints, coupled with our new ^{10}Be and *in situ* ^{14}C ages suggest that the western coast of Spitsbergen between Hornsund and Scottbreen deglaciated between ~18-16 ka, and that deglaciation of Isfjorden occurred much later with the fjord mouth deglaciating at ~14.3 ka. Initial retreat of the western SBIS margin appears to have occurred at ~23 ka followed by relatively variable and asynchronous retreat between the Isfjorden and Hornsund sectors of the SBIS, thus highlighting the dynamic nature in which ice sheets recede. Lastly, *in situ* ^{14}C measurements offer the ability to rectify ambiguous ^{10}Be-based datasets influenced by isotopic inheritance in order to extract key chronological information.

Acknowledgements

We are grateful for logistical support from the Polish Polar Station at Hornsund and two Arctic field grants to Endre Gjermundsen from the Svalbard Science Forum by the Norwegian Research Council. A portion of this work was performed under the auspices of the U.S. Department of Energy by the Lawrence Livermore National Laboratory under contracts DE-AC52-07NA27344. Fieldwork would not have been possible without the help of Ellinor Falkgjerdet, Lina Gislefoss and Carl Petter Nielsen. This is LDEO contribution #XXXX and LLNL-JRNL-743296.

Figure Captions

Figure 1. Spitsbergen with locations referred to in the text and the 21 ka ice limit from Hughes et al. (2015; dashed line). KE – Kapp Ekholm, H – Hornsund, and IF – Isfjorden. Previously published radiocarbon (cal ka BP) and ^{10}Be ages across Spitsbergen from previous studies constraining ice margin position are presented in two groups: 1) Ages that mark the initial timing of retreat or thinning of the ice margin from the LGM maximum extent (white ovals with black text), and 2) oldest coastal ages that constrain deglaciation following the LGM maximum extent and deglaciation of the present coastline (black ovals/white text). Location numbers are linked to Table 4; see Table 4 for sample details and references. Locations and ^{10}Be ages marked with stars and boxes are from this study. Isfjorden and Hornsund transects from Figure 4 are marked with black lines. Base and inset maps are from Jakobsson et al. (2012).

Figure 2. Ice margin constraints at Hornsund (Norwegian Polar Institute; toposvalbard.npolar.no/; collected in 2011). Individual ^{10}Be ages from bedrock are shown in black text with white boxes; up-fjord erratics on the Treskelen Peninsula are displayed in white text with black boxes. Only the mean *in situ* ^{14}C and ^{10}Be age from the Torbjørnsenfjellet (n = 5) and Wurmbrandegga (n = 6) elevation transects are shown (see Fig. 3). The minimum-limiting radiocarbon age just north of Hornsund is in green (U-2972; 12,100 $\pm$ 320 cal ka BP; Birkenmajer and Olsson, 1998; Table 4.).

Figure 3. Elevation transects in the Hornsund region. A) Field photograph of Torbjørnsenfjellet with sample locations B) Field photograph of Wurmbrandegga with sample locations. C) Comparison of paired ^{10}Be and *in situ* ^{14}C ages at Torbjørnsenfjellet, and the ^{10}Be-dated Wurmbrandegga elevation transect located ~12 km up-fjord from Torbjørnsenfjellet.

Figure 4. Measured ^{26}Al/^{10}Be ratios against ^{10}Be concentration at Torbjørnsenfjellet. Also plotted is the ^{14}C-corrected ^{26}Al/^{10}Be ratio for samples TORB-3 and TORB-4 using the average ^{14}C age of 17.4 $\pm$ 0.7 ka from the Torbjørnsenfjellet transect (i.e. the ratio at 17.4 ka). The corrected ratios for TORB-1 and TORB-2 result in values that overlap zero, which is suggestive of no previous sample exposure or burial. The corrected

ratio for TORB-5 also overlaps zero, which is due to subtracting more ^{26}Al than what was measured. However, the corrected ^{10}Be concentration in TORB-5 suggests a small amount of previous exposure.

Figure 5. A) Svalbard glaciation curve (Mangerud et al., 1998; Eccleshall et al., 2016). The timing of glacier advance has been tuned to coincide with the Marine Isotope Stage (MIS) that each advance is thought to correlate to as discussed in Eccleshall et al. (2016). MIS definitions are from Lisiecki and Raymo (2005). PIs-D: Phantomodden insterstadial D, G-E: Glaciation E, KEIs-F: Kapp Ekholm interstadial F, Ig-H: Interglaciation H. Shown are the modeled proof-of-concept ^{10}Be and *in situ* ^{14}C concentrations at 252 m asl (TORB-3) assuming that our Torbjørnsenfjellet sample sites become exposed and buried following the Svalbard glaciation curve and assuming a 'true' deglaciation age of 13.3 ka. The resulting *in situ* ^{14}C concentration equates to an exposure age of ~14.6 ka B) Retreat chronologies for the Hornsund and Isfjorden sectors of the SBIS compared to the NGRIP δ^{18}O record (North Greenland Ice Core Project Members, 2004) and a record of ice-rafted detritus and δ^{18}O (*N. pachyderma s.*) from core JM03-373PC2 located southwest of Hornsund (Rasmussen et al., 2007; Jessen et al., 2010; see location #2 on Fig. 1). Numbers between data points are the calculated net (minimum) ice-margin retreat rates using the age constraint midpoint. Symbols are larger than the uncertainties with the exception of the *in situ* ^{14}C-based Tobjornsenfjellet data point. JM03-373PC2 age model has been re-calibrated using CALIB 7.1 and a reservoir correction of 440 years (Stuiver et al., 2018; see Rasmussen et al., 2007 and Jessen et al., 2010 for details).

References

Balco G. 2011. Contributions and unrealized potential contributions of cosmogenic-nuclide exposure dating to glacier chronology, 1990-2010. *Quaternary Science Reviews* **30**: 3-27.

Balco G. 2017. Production rate calculations for cosmic-ray-muon-produced ^{10}Be and ^{26}Al benchmarked against geological calibration data. *Quaternary Geochronology* **39**: 150-173.

Balco G, Stone J, Lifton N, Dunai TJ. 2008. A simple, internally consistent, and easily accessible means of calculating surface exposure ages and erosion rates from Be-10 and Al-26 measurements. *Quaternary Geochronology* **3**: 174–195.

Balco G, Stone JOH, Sliwinski MG, Todd C. 2014. Features of the glacial history of the Transantarctic Mountains inferred from cosmogenic ^{26}Al ^{10}Be and ^{21}Ne concentrations in bedrock surfaces. *Antarctic Science* **26**: 708-723.

Balco G, Todd C, Huybers K, Campbell S, Vermeulen M, Hegland M, Goehring BM, Hillebrand TR. 2016. Cosmogenic-nuclide exposure ages from the Pensacola Mountains adjacent to the Foundation ice stream, Antarctica. *American Journal of Science* **316**: 542-577, doi: 10.2475/06.2016.02.

Birkenmajer K, Olsson IU. 1998. Radiocarbon-dated late Pleistocene and early Holocene marine shells at Werenskioldbreen, south Spitsbergen. *Bulletin of the Polish Academy of Sciences, Earth Sciences* **46**: 21-34.

Blaszczyk M, Jania JA, Kolondra L. 2013. Fluctuations of tidewater glaciers in Hornsund Fjord (Southern Svalbard) since the beginning of the 20th century. *Polish Polar Research* **34**: 327-352.

Briner JP, Lifton NA, Miller GH, Refsnider K, Anderson R, Finkel RC. 2014. Using *in situ* cosmogenic ^{10}Be, ^{14}C, and ^{26}Al to decipher the history of polythermal ice sheets on Baffin Island, Arctic Canada. *Quaternary Geochronology* **19**: 4-13, doi:10.1016/j.quageo.2012.11.005.

Briner JP, Goehring BM, Mangerud J, Svendsen JI. 2016. The deep accumulation of ^{10}Be at Utsira, southwestern Norway: Implications for cosmogenic nuclide exposure dating in peripheral ice sheet landscapes. *Geophysical Research Letters*: **43**, doi:10.1002/2016GL070100.

Cadman V. 1996. Glacimarine Sedimentation and Environments during the Late Weichselian and Holocene in the Bellsund Trough and Van Keulenfjorden. Thesis, *University of Cambridge*.

Chmeleff J, von Blanckenburg F, Kossert K, Jakob D. 2010. Determination of the ^{10}Be half-life by multicollector icp-ms and liquid scintillation counting. *Nuclear Instruments and Methods in Physics Research Section B: Beam Interactions with Materials and Atoms* **268**: 192-199.

Corbett L, Bierman PR, Graly JA, Neumann TA, Rood DH. 2013. Constraining landscape history and glacial erosivity using paired cosmogenic nuclides in Upernavik, northwest Greenland. *Geological Society of America Bulletin* **125**: 1539-1553.

Eccleshall SV, Hormes A, Hovland A, Preusser F. 2016. Constraining the chronology of Pleistocene glaciations on Svalbard: Kapp Ekholm re-visited. *Boreas* **45**: 790-803.

Elverhøi A, Anders ES, Dokken T, Hebblen D, Spielhagen R, Svendsen J, Sørflaten M, Rørnes A, Hald M, Forsberg CS. 1995. The growth and decay of the Late Weichselian ice sheet in western Svalbard and adjacent areas based on provenance studies of marine sediments. *Quaternary Research* **44**: 303-316.

Forwick M, Vorren T-O. 2007. Holocene mass-transport activity and climate in outer Isfjorden, Spitsbergen: marine and subsurface evidence. *The Holocene* **17**: 707-716.

Gjermundsen EF, Briner JP, Akçar N, Salvigsen O, Kubik P, Gantert N, Hormes A. 2013. Late Weichselian local ice dome configuration and chronology in Northwestern Svalbard: early thinning, late retreat. *Quaternary Science Reviews* **72**: 112-127.

Gjermundsen EF, Briner JP, Akçar N, Foros J, Kubik PW, Salvigsen O, Hormes A. 2015. Minimal erosion of Arctic alpine topography during late Quaternary glaciation. *Nature Geoscience* **8**: 789-782, doi:10.1038/ngeo2524.

Goehring BM, Schaefer JM, Schluechter C, Lifton NA, Finkel RC, Timothy Jull AJ, Akçar N, Alley RB. 2011. The Rhone Glacier was smaller than today for most of the Holocene. *Geology* **39**: 679-682, doi:10.1130/G32145.1.

Goehring BM, Schimmelpfennig I, Schaefer JM. 2014. Capabilities of the Lamont-Doherty Earth Observatory in situ ^{14}C extraction laboratory updated. *Quaternary Geochronology* **19**: 194-197.

Granger DE, Lifton NA, Willenbring JK. 2013. A cosmic trip: 25 years of cosmogenic nuclides in geology. *Geological Society of America Bulletin* **125**: 1379-1402.

Håkansson L, Alexanderson H, Hjort C, Möller P, Briner JP, Aldahan A, Possnert G. 2008. Late Pleistocene glacial history of Jameson Land, central East Greenland, derived from cosmogenic ^{10}Be and ^{26}Al exposure dating. *Boreas* **38**: 244-260.

Hogan KA, Dowdeswell JA, Noormets R, Evans J, O'Cofaigh C. 2010. Evidence for full-glacial flow and retreat of the Late Weichselian Ice Sheet from the waters around Kong Karls Land, eastern Svalbard. *Quaternary Science Reviews* **29**: 3563-3582.

Hormes A, Akçar N, Kubik PW. 2011. Cosmogenic radionuclide dating indicates ice-sheet configuration during MIS 2 on Nordaustlandet, Svlabard. *Boreas* **40**: 636-649.

Hormes A, Gjermundsen EF, Rasmussen TL. 2013. From mountain top to the deep sea – Deglaciation in 4D of the northwestern Barents Sea ice sheet. *Quaternary Science Reviews* **75**: 78-99.

Hughes ALC, Gyllencreutz R, Lohne ØS, Mangerud J, Svendsen JI. 2015. The last Eurasian ice sheets – a chronological database and time-slice reconstruction, DATED-1. *Boreas* **45**: 1-45, doi: 10.1111/bor.12142.

Ingólfsson O, Landvik JY. 2013. The Svalbard-Barents Sea ice-sheet – Historical, current and future perspectives. *Quaternary Science Reviews* **64**: 33-60.

Ivy-Ochs S, Briner JP. 2014. Dating disappearing ice with cosmogenic nuclides. *Elements* **10**: 351-356.

Jakobsson M, Mayer LA, Coakley B, Dowdeswell JA, Forbes S, Fridman B, Hodnesdal H, Noormets R, Pedersen R, Rebesco M, Schenke HW, Zarayskaya Y, Accettella AD, Armstrong A, Anderson RM, Bienhoff P, Camerlenghi A, Church I, Edwards M, Gardner JV, Hall JK, Hell B, Hestvik OB, Kristoffersen Y, Marcussen C, Mohammad R, Mosher D, Nghiem SV, Pedrosa MT, Travaglini PG, Weatherall P. 2012. The International Bathymetric Chart of the Arctic Ocean (IBCAO) Version 3.0. *Geophysical Research Letters doi:* 10.1029/2012GL052219.

Jessen SP, Rasmussen TL, Nielsen T, Solheim A. 2010. A new Late Weichselian and Holocene marine chronology for the western Svalbard slope 30,000 – 0 cal years BP. *Quaternary Science Reviews* **29**: 1301-1312.

Johnson JS, Smith JA, Schaefer JM, Young NE, Goehring BM, Hillenbrand C-D, Lamp JL, Finkel RC, Gohl K. 2017. The last glaciation of Bear Peninsula, central Amundsen Sea Embayment of Antarctica: Constraints on timing and duration revealed by in situ cosmogenic ^{14}C and ^{10}Be dating. *Quaternary Science Reviews* **178**: 77-88.

Lal D. 1991. Cosmic ray labeling of erosion surfaces: *in situ* nuclide production rates and erosion models. *Earth and Planetary Science Letters* **104**: 424-429.

Koç N, Klitgaard-Kristensen D, Hasle K, Forsberg CK, Solheim A. 2002. Late glacial palaeoceanography of Hinlopen Strait, northern Svalbard. *Polar Research* **21**: 307-314.

Landvik JY, Bondevik S, Elverhøi A, Fjeldskaar W, Mangerud J, Salvigsen O, Siegert MJ, Svendsen JI, Vorren TO. 1998. The last glacial maximum of Svalabrd and the Barents Sea area: Ice sheet extent and configuration. *Quaternary Science Reviews* **17**: 43-75.

Landvik JY, Brook EJ, Gualtieri L, Raisbeck G, Salvigsen O, Yiou F. 2003. Northwest Svalbard during the last glaciation: ice-free areas existed. *Geology* **31**: 905-908.

Landvik JY, Ingolfsson O, Mienert J, Lehman SJ, Solheim A, Elverhøi A, Ottesen D. 2005. Rethinking

Late Weichselian ice-sheet dynamics in coastal NW Svalbard. *Boreas* **34**: 7-24.

Landvik JY, Brook EJ, Gualtieri L, Linge H, Raisbeck G, Salvigsen O, Yiou F. 2013. ^{10}Be exposure age constraints on the Late Weichselian ice-sheet geometry and dynamics in inter-ice-stream areas, western Svalbard. *Boreas* **42**: 43-56.

Landvik JY, Alexanderson H, Henriksen M, Ingólfsson O. 2014. Landscape imprints of changing glacial regimes during ice-sheet build-up and decay: a conceptual model from Svalbard. *Quaternary Science Reviews* **92**: 258-268.

Lifton NA, Timothy Jull AJ, Quade J. 2001. A new extraction technique and production rate estimate for in situ cosmogenic ^{14}C in quartz. *Geochimica et Cosmochimica Acta* **65**: 1953-1969.

Lisecki LE, Raymo ME. 2005. A Pliocene-Pleistocene stack of 57 globally distributed benthic δ^{18}O records. *Paleoceanography,* doi:10.1029/2004PA001071.

Mangerud J, Svendsen JI. 1990. Deglaciation chronology inferred from marine sediments in a proglacial lake basin, western Spitsbergen. *Boreas* **19**: 249-272.

Mangerud J, Bondevik S, Gulliksen S, Hufthammer KA, Hoisaeter T. 2006. Marine ^{14}C reservoir ages for 19th century whales and molluscs from the North Atlantic. *Quaternary Science Reviews* **25**: 3228-3245.

Nishiizumi K, Imamura M, Caffee MW, Southon JR, Finkel RC, McAninch J. 2007. Absolute calibration of ^{10}Be AMS standards. *Nuclear Instruments and Methods in Physics Research B* **258**: 403-413.

North Greenland Ice Core Project members. 2004. High-resolution record of Northern Hemisphere climate extending into the last interglacial period. *Nature* **431**: 147-151.

Patton H, Hubbard A, Andreassen K, Winsborrow M, Stroeven AP. 2016. The build-up, configuration, and dynamical sensitivity of the Eurasian ice-sheet complex to Late Weichselian climatic and oceanic forcing. *Quaternary Science Reviews* **153**: 97-121.

Phillips W, Briner JP, Gislefoss L, Linge H, Koffman T, Fabel D, Xu S, Hormes A. 2017. Late Holocene glacier activity at inner Hornsund and Scottbreen, southern Svalbard. *Journal of Quaternary Science* **32**: 501-515.

Rasmussen TL, Thomsen E, Slubowska MA, Jessen S, Solheim A, Koç N. 2007. Paleoceanographic evolution of the SW Svalbard margin (76 degrees N) since 20,000 ^{14}C yr BP. *Quaternary Research* **67**: 100-114.

Salvigsen O, Elgersma A. 1991. Radiocarbon Dated Raised Beaches in Northwestern Wedel Jarlsberg Land, Spitsbergen, Svalbard. *Wyprawy Geograficzne na Spitsbergen*: 9-16.

Schaefer JM, Denton GH, Kaplan M, Putnam A, Finkel RC, Barrell DJA, Andersen BG, Schwartz R, Mackintosh A, Chinn T, Schlüchter C. 2009. High-frequency Holocene glacier fluctuations in New Zealand differ from the Northern signature. *Science* **324**: 622-625.

Staiger J, Gosse J, Toracinta R, Oglesby B, Fastook J, Johnson JV. 2007. Atmospheric scaling of cosmogenic nuclide production: climate effect. *Journal of Geophysical Research* **112**: B02205.

Stokes CR, and 25 others. 2015. On the reconstruction of palaeo-ice sheets: Recent advances and future challenges. *Quaternary Science Reviews* **125**: 15-49.

Stone JO. 2000. Air pressure and cosmogenic isotope production. *Journal of Geophysical Research* **105**: 23,753-23,759.

Stuiver M, Reimer PJ, Reimer RW. 2018. *CALIB 7.1 [WWW program] at http://calib.org*, accessed 2018-5-10.

Svendsen JI, Mangerud J, Elverhøi A, Solheim A, Schüttenhelm RTE. 1992. The Late Weichselian glacial maximum on western Spitsbergen inferred from offshore sediment cores. *Marine Geology* **104**: 1-17.

Svendsen JI, Elverhøi A. Mangerud J. 1996. The retreat of the Barents Sea Ice Sheet on the western Svalbard margin. *Boreas* **25**: 244-256.

Svendsen JI, and 29 others. 2004. Late Quaternary ice sheet history of northern Eurasia. *Quaternary Science Reviews* **23**: 1229-1271.

Ullman DJ, Carlson AE, LeGrande AN, Anslow FS, Moore AK, Caffee M, Syverson KM, Licciardi JM. 2015. Southern Laurentide ice-sheet retreat synchronous with rising boreal summer insolation. *Geology* **43**: 23-26, doi:10.1130/G36179.1.

Young NE, Briner JP, Axford Y, Csatho B, Babonis GS, Rood DH, Finkel RC. 2011. Response of a marine-terminating Greenland outlet glacier to abrupt cooling 8200 and 9300 years ago. *Geophysical Research Letters* **38**: L24701, doi:10.1029/2011GL049639.

Young NE, Schaefer JM, Briner JP, Goehring BM. 2013. A ^{10}Be production-rate calibration for the Arctic. *Journal of Quaternary Science* **28**: 515-526.

Young NE, Schaefer JM, Goehring BM, Lifton N, Schimmelpfennig I, Briner JP. 2014. West Greenland and global in situ ^{14}C production-rate calibrations. *Journal of Quaternary Science* **29**: 401-406.

Young NE, Briner JP, Maurer J, Schaefer JM. 2016. ^{10}Be measurements in bedrock constrain erosion beneath the Greenland Ice Sheet margin. *Geophysical Research Letters* **43**: doi: 10.1002/ 2016GL070258.


15° E
21 ka
80° N
80° N
Nordaustlandet
Spitsbergen
KE
IF
H
Edgeøya
77°30' N
77°30' N
17.7 Scottbreen
15.9 Fløyfjellet
15.9 Torellbreen
17.4 Torbjornsenfjellet
13.0 Treskelen
13.3 Wurmbrandegga
Fig. 2
50 km
15° E
33 16.5
32 16.8
13 26.7
14 28.3
15 22.0
11 17.9
10 19.3
9 21.8
12 21.7
31 15.6
8 25.0
30 16.9
29 16.2
28 16.5
7 20.3
26 11.0
27 11.1
25 12.4
19 17.9
20 14.4
22 14.3
23 12.4
24 12.2
6 23.2
21 14.6
5 18.8
18 13.7
4 19.8
17 12.1
3 23.0
16 11.7
2 22.7
1 19.6

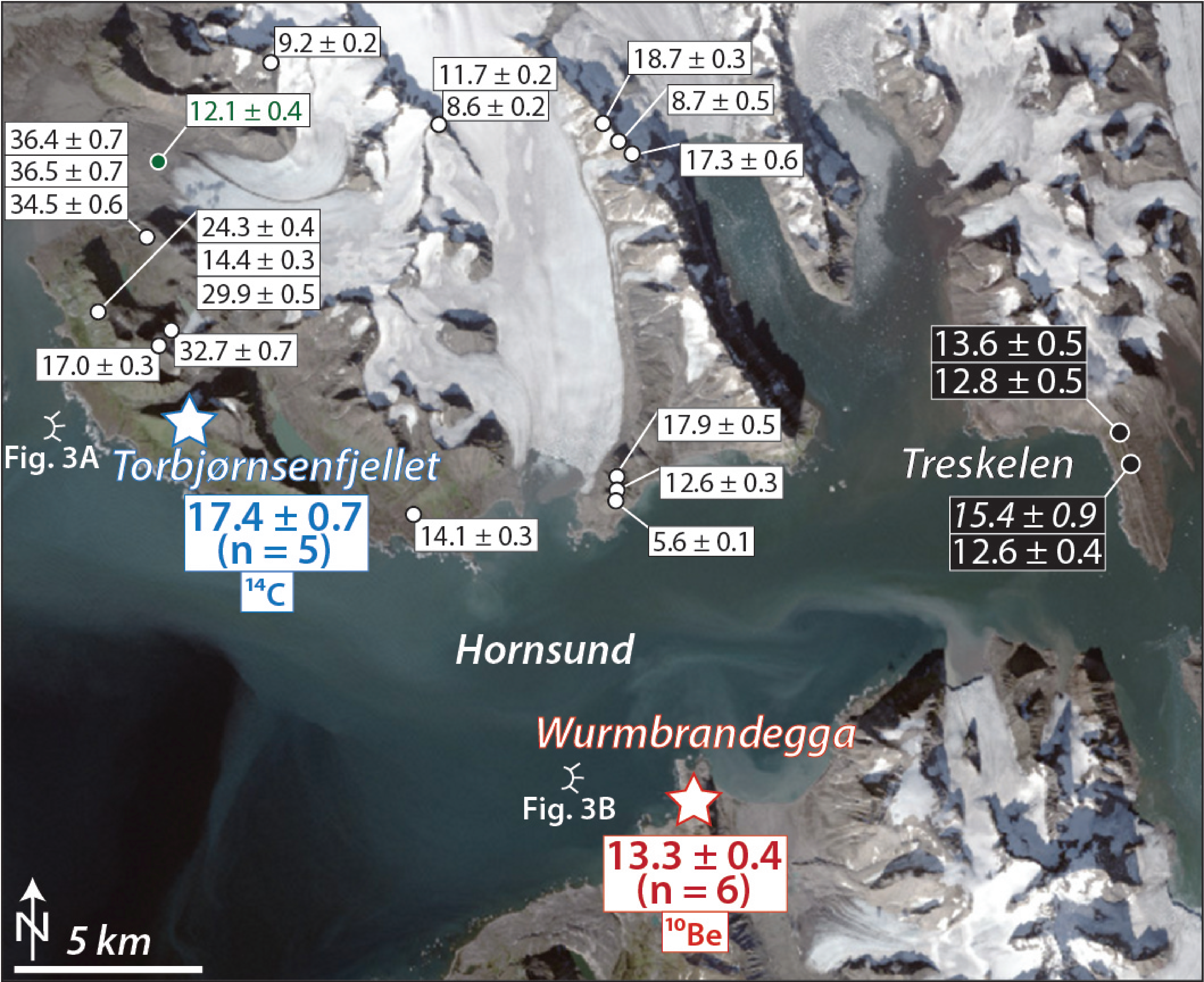

9.2 ± 0.2
12.1 ± 0.4
11.7 ± 0.2
8.6 ± 0.2
18.7 ± 0.3
8.7 ± 0.5
17.3 ± 0.6
36.4 ± 0.7
36.5 ± 0.7
34.5 ± 0.6
24.3 ± 0.4
14.4 ± 0.3
29.9 ± 0.5
32.7 ± 0.7
17.0 ± 0.3
13.6 ± 0.5
12.8 ± 0.5
17.9 ± 0.5
12.6 ± 0.3
5.6 ± 0.1
14.1 ± 0.3
15.4 ± 0.9
12.6 ± 0.4
Fig. 3A
Torbjørnsenfjellet
17.4 ± 0.7
(n = 5)
14C
Treskelen
Hornsund
Wurmbrandegga
Fig. 3B
13.3 ± 0.4
(n = 6)
10Be
N
5 km

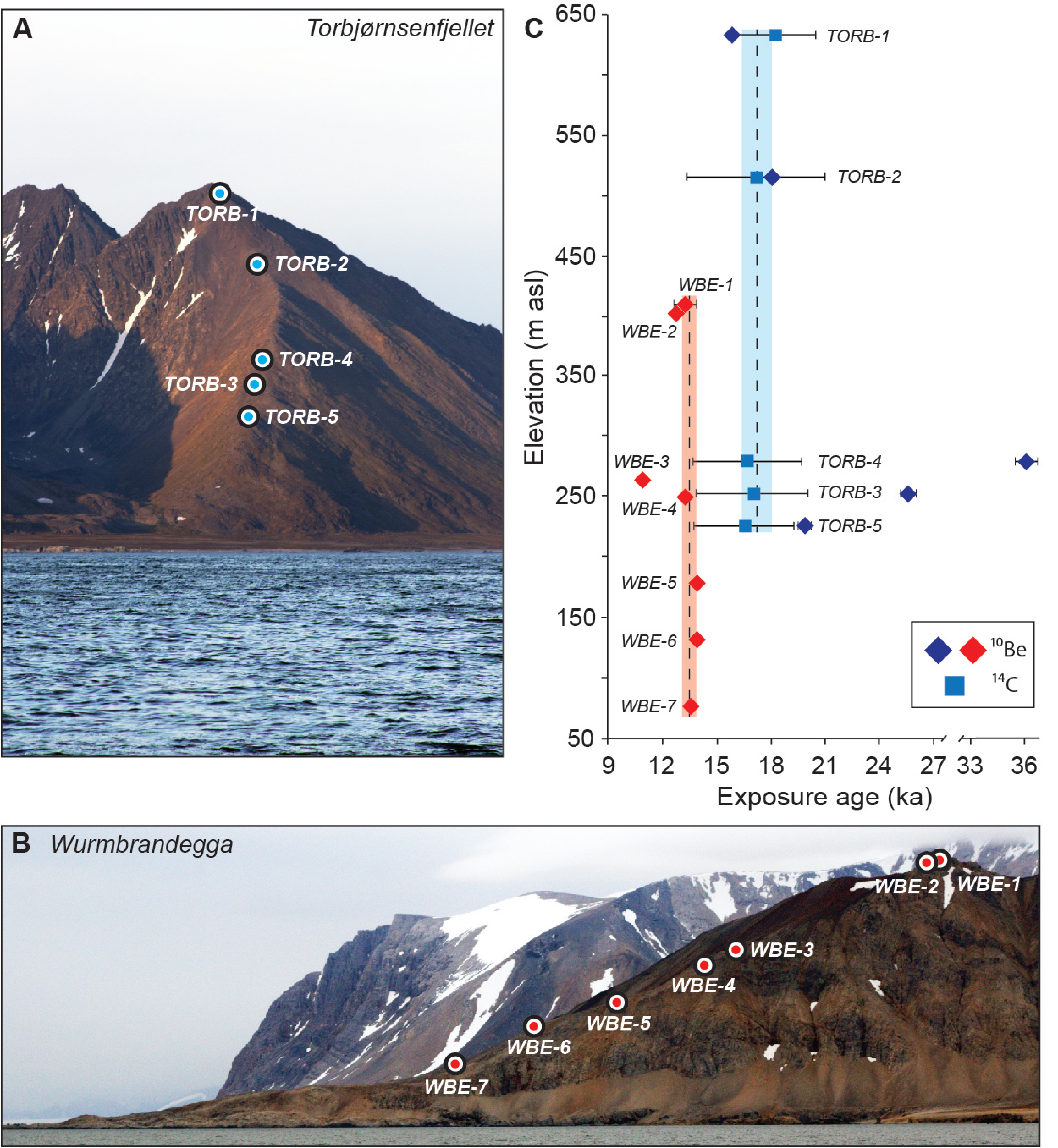
A
Torbjørnsenfjellet
TORB-1
TORB-2
TORB-4
TORB-3
TORB-5
C
650
550
450
350
250
150
50
Elevation (m asl)
9
12
15
18
21
24
27
33
36
Exposure age (ka)
WBE-1
WBE-2
WBE-3
WBE-4
WBE-5
WBE-6
WBE-7
10Be
14C
B
Wurmbrandegga

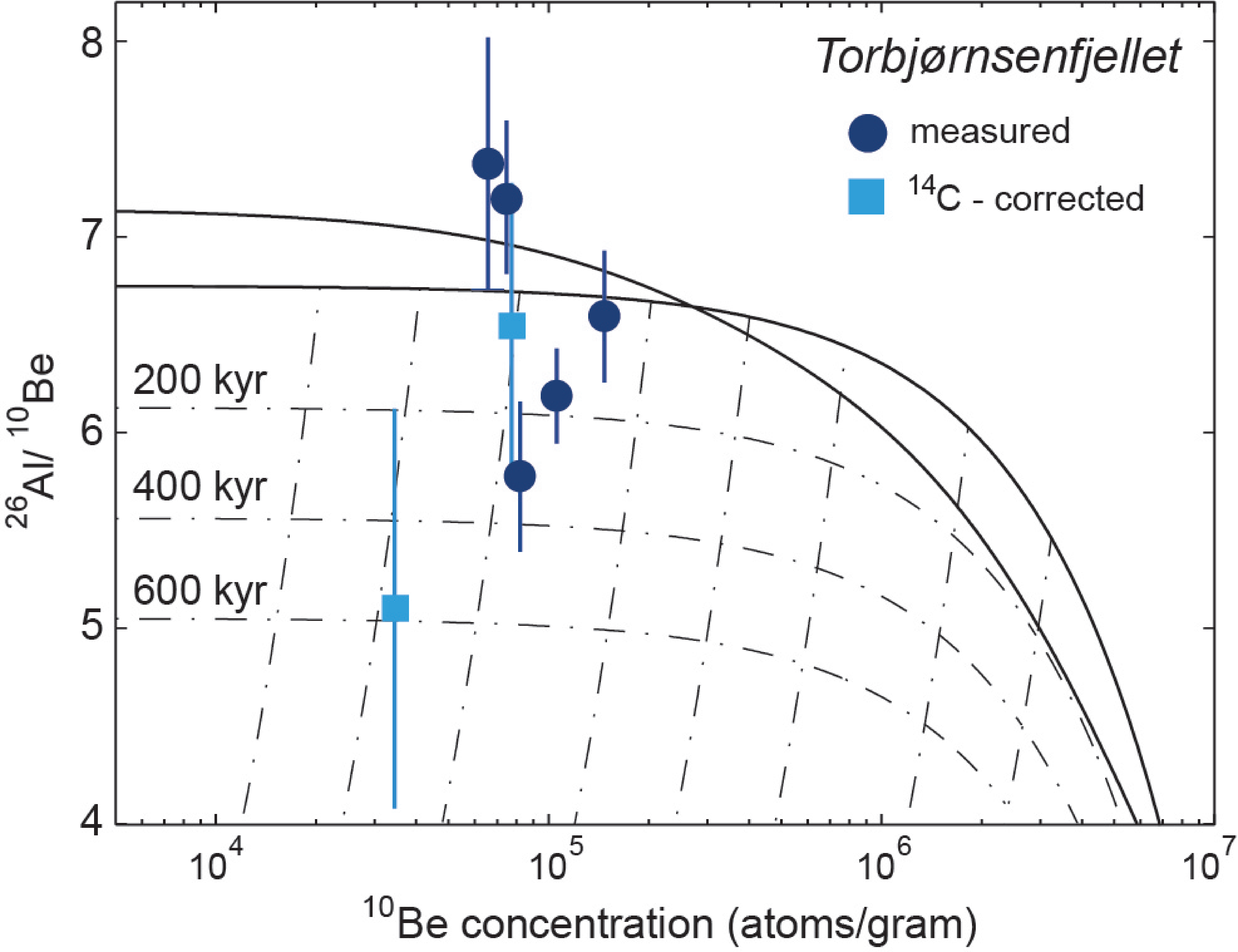
Torbjørnsenfjellet
measured
14C - corrected
200 kyr
400 kyr
600 kyr
8
7
6
5
4
26Al/ 10Be
10^4
10^5
10^6
10^7
10Be concentration (atoms/gram)

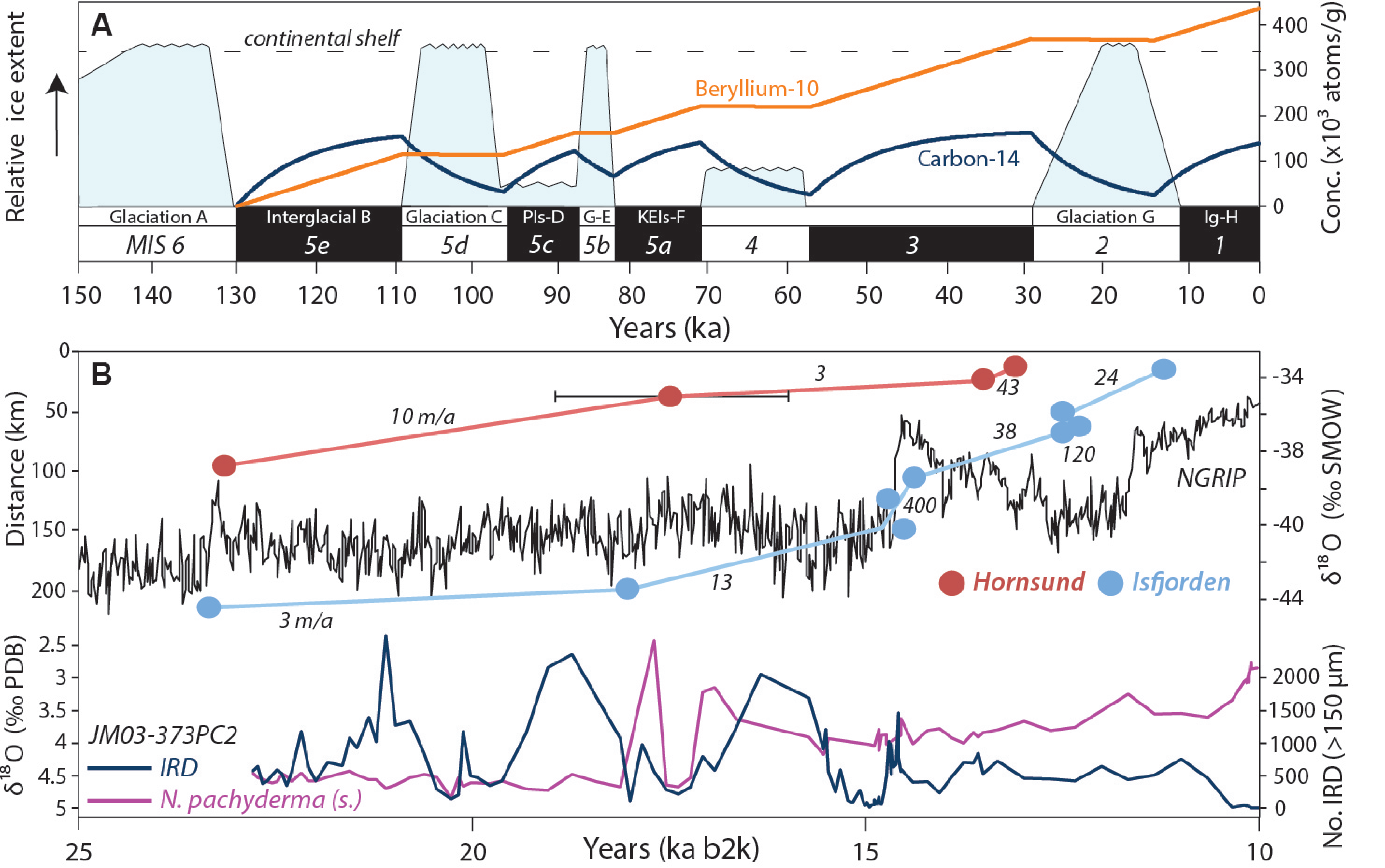
A
continental shelf
Relative ice extent
Beryllium-10
Carbon-14
Conc. ($x10^3$ atoms/g)
Glaciation A
Interglacial B
Glaciation C
PIs-D
G-E
KEIs-F
Glaciation G
Ig-H
MIS 6
5e
5d
5c
5b
5a
4
3
2
1
Years (ka)
B
Distance (km)
$\delta^{18}O$ (‰ SMOW)
10 m/a
3
43
24
38
120
400
13
3 m/a
NGRIP
Hornsund
Isfjorden
$\delta^{18}O$ (‰ PDB)
No. IRD (>150 µm)
JM03-373PC2
IRD
N. pachyderma (s.)
Years (ka b2k)

Table 1. Sample information and ^{10}Be and ^{26}Al data

Sample	Sample type	Latitude (DD)	Longitude (DD)	Elevation (m asl)	Thickness (cm)	Shielding correction	Quartz (g)	^{9}Be carrier added (g)	Carrier conc. (ppm)	$^{10}Be/^{9}Be$ ratio ± 1σ (10^{-13})[a]	$^{26}Al/^{27}Al$ ratio ± 1σ (10^{-13})	^{10}Be conecentration (atoms g^{-1})[c]	^{10}Be uncertainty (atoms g^{-1})	^{10}Be age - Lm (ka)	^{26}Al conecentration (atoms g^{-1})	^{26}Al uncertainty (atoms g^{-1})	^{26}Al age - Lm (ka)	$^{26}Al/^{10}Be$	Laboratory
Scottbreen																			
SCO-14-12	bedrock	77.5538	14.4423	142	1.0	0.9955	39.9946	0.6092	372.5	2.4648 ± 0.0638		92616	2421	18.8 ± 0.5					Buffalo
SCO-14-13	bedrock	77.5557	14.4447	119	2.0	0.9973	30.4387	0.6082	372.5	1.7251 ± 0.0325		85543	1629	17.9 ± 0.3					Buffalo
SCO-14-14	bedrock	77.5563	14.4438	104	1.0	0.9982	35.0566	0.6072	372.5	1.8143 ± 0.0343		77270	1488	16.3 ± 0.3					Buffalo
SCO-14-15	bedrock	77.5563	14.4436	115	2.0	0.9982	20.1923	0.6106	372.5	1.1563 ± 0.0228		84618	1738	17.8 ± 0.4					Buffalo
														17.7 ± 1.0					
Fløyfjellet																			
FLO-14-01	bedrock	77.4124	14.0924	265	2.0	0.9968	15.0139	0.1818	1037	1.0766 ± 0.0174		90104	1962	16.2 ± 0.4					LDEO
FLO-14-02	bedrock	77.4123	14.0880	252	2.0	0.9996	12.0044	0.1816	1037	0.8357 ± 0.0157		87311	2063	15.9 ± 0.4					LDEO
FLO-14-03	bedrock	77.4133	14.0883	234	2.0	0.9988	14.9806	0.1815	1037	0.9870 ± 0.0227		82634	2392	15.3 ± 0.4					LDEO
FLO-14-04	bedrock	77.4141	14.0867	229	2.0	0.9985	15.2578	0.1818	1037	1.0567 ± 0.0198		87026	2053	16.2 ± 0.4					LDEO
														15.9 ± 0.4					
Torellbreen																			
55-PLO-1	bedrock	77.2604	15.1582	812	5.0	0.9469	15.1596	0.6073	372.5	1.5003 ± 0.0420		149906	4185	17.3 ± 0.5					Buffalo
70-ORV-1	bedrock	77.3097	14.6887	637	2.0	0.9774	13.4797	0.6071	372.5	1.6248 ± 0.0322		179656	3614	*23.0 ± 0.5*					Buffalo
70-ORV-2	bedrock	77.3097	14.6887	637	2.0	0.9998	20.0332	0.6064	372.5	1.7188 ± 0.0320		127826	2408	16.0 ± 0.3					Buffalo
70-ORV-3	bedrock	77.3099	14.6775	587	2.0	0.9992	20.0732	0.6054	372.5	1.4715 ± 0.0273		108796	2049	14.3 ± 0.3					Buffalo
														15.9 ± 1.5					
Hornsund nunataks/bedrock																			
70-NORD-1	bedrock	77.0939	15.6894	751	2.0	0.9999	20.2885	0.6065	372.5	2.2582 ± 0.0367		166380	2734	18.7 ± 0.3					Buffalo
55-VAR-1	bedrock	77.0890	15.7062	698	5.0	0.9999	5.1862	0.6073	372.5	0.2472 ± 0.0144		72048	4209	8.7 ± 0.5					Buffalo
55-VAR-2	bedrock	77.0885	15.7082	680	4.5	0.9967	13.4856	0.6076	372.5	1.2506 ± 0.0449		140255	5036	17.3 ± 0.6					Buffalo
66-SLY-1	bedrock	77.0939	15.5151	656	2.32	1.0000	26.0395	0.6122	372.5	1.6440 ± 0.0290		95058	1855	11.7 ± 0.2					Buffalo
65-SLY-2	bedrock	77.0939	15.5152	657	1.47	1.0000	19.6358	0.6106	372.5	0.9339 ± 0.0177		70586	1395	8.6 ± 0.2					Buffalo
70-BARA-1	bedrock	77.1086	15.3442	868	2.0	1.0000	27.8512	0.6112	372.5	1.7000 ± 0.0301		90701	1689	9.2 ± 0.2					Buffalo
68-BRATT-1	bedrock	77.0674	15.2118	110	2.43	1.0000	35.7727	0.6066	372.5	4.0805 ± 0.0793		170651	3361	36.4 ± 0.7					Buffalo
66-BRATT-2	bedrock	77.0674	15.2114	110	0.94	1.0000	40.0399	0.6127	372.5	4.5705 ± 0.0881		173339	3347	36.5 ± 0.7					Buffalo
66-BRATT-3	bedrock	77.0674	15.2115	109	1.26	1.0000	29.0404	0.6116	372.5	3.1365 ± 0.0559		163393	3007	34.5 ± 0.6					Buffalo
66-GUL-1	bedrock	77.0522	15.1845	548	1.27	1.0000	27.0770	0.6123	372.5	3.2105 ± 0.0546		179608	3156	24.3 ± 0.4					Buffalo
66-GUL-2	bedrock	77.0535	15.1838	580	1.78	1.0000	40.1016	0.6104	372.5	2.9056 ± 0.0522		109342	2034	14.4 ± 0.3					Buffalo
67-GUL-3	bedrock	77.0515	15.1852	526	1.47	1.0000	23.4779	0.6092	372.5	3.3705 ± 0.0541		215620	3495	29.9 ± 0.5					Buffalo
67-Jahn-1	bedrock	77.0440	15.2406	600	2.0	1.0000	30.1245	0.6104	372.5	2.6393 ± 0.0449		131504	2262	17.0 ± 0.3					Buffalo
68-JAHN-2	bedrock	77.0461	15.2449	510	2.0	1.0000	12.4195	0.6068	372.5	1.9395 ± 0.0378		231315	4600	32.7± 0.7					Buffalo
FAN-14-01	bedrock	77.0103	15.7024	388	3.0	1.0000	10.8458	0.1804	1037	0.6877 ± 0.0131		78935	1865	12.6 ± 0.3					LDEO
FAN-14-02	bedrock	77.0145	15.7017	397	3.0	0.9970	15.1240	0.1820	1037	1.3551 ± 0.0272		112784	2976	17.9 ± 0.5					LDEO
FAN-14-03	bedrock	77.0097	15.7015	380	3.0	0.9990	14.6232	0.1814	1037	0.4088 ± 0.0095		34889	898	5.6 ± 0.1					LDEO
ARD-01	bedrock	77.0068	15.4910	61	2.89	0.9965	20.3730	0.1829	1037	1.0092 ± 0.0193		62610	1479	14.1 ± 0.3					LDEO
Torbjørsenfjellet																			
14TORB-1	bedrock	77.0265	15.2679	633	1.87	0.9773	17.5809	0.1824	1024	1.7664 ± 0.0285	4.3881 ± 0.3316	124966	2031	16.0 ± 0.3	921682	79016	17.6 ± 1.5	7.38 ± 0.64	LDEO
14TORB-2	bedrock	77.0263	15.2601	515	3.04	0.9781	16.7093	0.1819	1024	1.7027 ± 0.0276	3.8344 ± 0.1548	126381	2068	18.3 ± 0.3	910442	46629	19.6 ± 1.0	7.20 ± 0.39	LDEO
14TORB-3	bedrock	77.0271	15.2312	252	2.45	0.9951	31.2907	0.1828	1024	3.5131 ± 0.0538	7.9293 ± 0.2429	140213	2153	25.8 ± 0.4	866472	31816	23.7 ± 0.9	6.18 ± 0.25	LDEO
14TORB-4	bedrock	77.0273	15.2343	279	1.53	0.9910	14.8254	0.1819	1024	2.4246 ± 0.0394	4.1403 ± 0.1666	203065	3313	36.3 ± 0.6	1339280	65019	35.8 ± 1.8	6.60 ± 0.34	LDEO
14TORB-5	bedrock	77.0276	15.2281	225	2.09	0.9936	36.0443	0.1821	1024	3.0806 ± 0.0516	6.3974 ± 0.3634	106472	1789	20.1 ± 0.3	614729	39491	17.2 ± 1.1	5.77 ± 0.38	LDEO
Wurmbrandegga																			
WBE-14-01	bedrock	76.9349	15.7808	412	2.0	1.0000	25.7482	0.6087	372.5	0.8823 ± 0.0360		85508	3646	13.2 ± 0.6					Buffalo
WBE-14-02	bedrock	76.9350	15.7805	406	2.0	1.0000	25.1815	0.6075	372.5	0.8342 ± 0.0160		81229	1732	12.7 ± 0.3					Buffalo
WBE-14-03	bedrock	76.9377	15.7748	260	2.0	0.9880	23.7882	0.6080	372.5	1.0545 ± 0.0230		59715	1418	10.9 ± 0.3					Buffalo
WBE-14-04	bedrock	76.9380	15.7745	248	2.0	0.9727	30.3079	0.6063	372.5	1.2143 ± 0.0212		70532	1348	13.2 ± 0.3					Buffalo
WBE-14-05	bedrock	76.9392	15.7718	181	2.0	0.9883	30.6524	0.6105	372.5	1.1370 ± 0.0194		69812	1316	13.8 ± 0.3					Buffalo
WBE-14-06	bedrock	76.9404	15.7702	133	2.0	0.9885	15.0869	0.6043	372.5	1.3564 ± 0.0276		65557	1419	13.7 ± 0.3					Buffalo
WBE-14-07	bedrock	76.9414	15.7680	78	2.0	0.9884	15.0632	0.6071	372.5	1.2637 ± 0.0238		60686	1234	13.4 ± 0.3					Buffalo
Treskelen																			
TR-01	erratic	77.0227	16.2057	156	2.6	0.9619	20.2170	0.12670	1664	0.957 ± 0.0326		64813	2462	13.6 ± 0.5					SUERC
TR-02	erratic	77.0227	16.2055	156	3.4	0.9922	28.8390	0.12660	1664	1.3057 ± 0.0511		62423	2650	12.8 ± 0.5					SUERC
TR-04	erratic	77.0160	16.2162	111	1.9	0.9981	16.5260	0.12810	1664	0.8705 ± 0.0477		72734	4247	15.4 ± 0.9					SUERC
TR-05	erratic	77.0161	16.2160	110	1.4	0.9979	25.5210	0.12710	1664	1.1076 ± 0.0349		59853	2117	12.6 ± 0.4					SUERC

All ages are calculated using version 3 of the CRONUS calculator code (Balco et al., 2008, Balco, 2017), the 'Arctic' ^{10}Be production rate (Young et al., 2013), standard atmosphere and pressure 'std', a rock density of 2.65 g cm-3, and assumes no erosion.

a - Samples processed at Buffalo and LDEO were measured at Lawrence Livermore National Laboratory - Center for Accelerator Mass Spectrometry. Samples processed at SUREC were measured at SUERC AMS Laboratory. All ratios are reported relative to 07KNSTD with a reported ratio of 2.85×10^{-12} using a ^{10}Be half-life of 1.36×10^{6} years (Nishiizumi et al., 2007).

b - ^{10}Be concentrations are blank corrected using batch-specific process blanks. LDEO samples are blank corrected using values of 8259 ± 3148 atoms (TORB samples) and 3842 ± 539 atoms (n = 2; FLO, FAN, ARD samples); ^{10}Be concentrations for all SUERC samples are blank corrected using a value of 37999 ± 537 atoms; Buffalo samples are blank corrected suing values of 48599 ± 5588 atoms (SCO-13, SCO-15, GUL-3, JAHN-1 samples), 33523 ± 9022 atoms (ORV-1, ORV-2, ORV-3, NORD-1 samples), 56575 ± 24289 atoms (BRATT-1, JAHN-2 samples), 29873 ± 19444 atoms (BRATT-2, BRATT-3, GUL-1, GUL-2, SLY-1 samples), 33430 ± 5180 atoms (SCO-12, SCO-14, SLY-2 samples), 60094 ± 10954 atoms (BARA-1, WBE-03, WBE-04, WBE-05, WBE-06, WBE-07 samples), and 37093 ± 9868 atoms (WBE-01 and WBE-02 samples).

Table 2. *In situ* ^{14}C extraction details

Sample	Date extracted	Quartz (g)	V_{CO2} (cc STP)	V_{dilute} (cc STP)	CAMS #
14TORB-1	########	5.1234	0.2576 ± 0.0030	1.5901 ± 0.0184	170000
14TORB-2	########	3.4877	0.4839 ± 0.0056	1.8295 ± 0.0211	173883
14TORB-3	########	5.0427	0.7704 ± 0.0089	1.4295 ± 0.0165	170152
14TORB-4	########	5.0307	0.3336 ± 0.0038	1.6875 ± 0.0194	173884
14TORB-5	########	5.1089	0.5360 ± 0.0062	0.9921 ± 0.0115	173356

All samples are blank corrected using a LDEO long-term value of 112.55 ± 36.83 x 10^3 ^{14}C

F_m measured	^{14}C blank-correted (atoms g^{-1})	^{14}C age - Lm (ka)	^{14}C age - LSD (ka)
0.0259 ± 0.0002	208248 ± 8111	18.5 ± 2.7	19.1 ± 2.9
0.0153 ± 0.0002	183882 ± 12146	17.6 ± 4.0	18.0 ± 4.3
0.0214 ± 0.0002	146890 ± 7942	17.3 ± 3.2	17.3 ± 3.2
0.0186 ± 0.0001	149829 ± 8358	16.9 ± 3.1	16.9 ± 3.1
0.0298 ± 0.0003	141823 ± 7643	16.7 ± 2.9	16.6 ± 2.9

: atoms (n=23)

Table 3a. *In situ* ^{14}C blank data

Sample	V_{CO2} (cc STP)	V_{dilute} (cc STP)	CAMS #	F_m measured	^{14}C (10^3 atoms)
Blank 11-20-14	0.01643 ± 0.00019	1.446 ± 0.017	168812	0.0048 ± 0.0001	107.03 ± 13.60
Blank 1-15-15	0.01295 ± 0.00015	1.391 ± 0.016	168813	0.0048 ± 0.0001	100.87 ± 13.18
Blank 3-10-15	0.01202 ± 0.00014	1.351 ± 0.015	169702	0.0061 ± 0.0001	153.24 ± 12.92
Blank 4-17-15	0.01346 ± 0.00016	1.424 ± 0.016	170151	0.0045 ± 0.0001	89.66 ± 13.48
Blank 9-16-15	0.01318 ± 0.00015	1.373 ± 0.016	172629	0.0063 ± 0.0001	164.18 ± 13.17
Blank 3-2-16	0.01401 ± 0.00016	1.403 ± 0.016	173886	0.0040 ± 0.0001	67.01 ± 13.22

We report all blank measurements completed since November 2014. The previous LDEO long-term blank was 118.09 ± 39.28 x 10^3 ^{14}C atoms and included blanks up to Septmeber 2013 (Young et al., 2014). The updated LDEO long-term blank value that includes the above measurements is 112.55 ± 36.83 x 10^3 ^{14}C atoms (n=23).

Table 3b. LDEO CRONUS-A *in situ* ^{14}C data

Sample	Quartz (g)	V_{CO2} (cc STP)	V_{dilute} (cc STP)	CAMS #	F_m measured	^{14}C (10^3 atoms g^{-1})
CRONUS-A-3-24-15	4.8795	0.1122 ± 0.0013	1.470 ± 0.017	169935	0.0826 ± 0.0003	735.89 ± 12.27
CRONUS-A-4-16-16	3.6393	0.0553 ± 0.0006	1.439 ± 0.017	173885	0.0618 ± 0.0004	706.23 ± 14.53
CRONUS-A-5-19-16	3.6502	0.0512 ± 0.0006	1.423 ± 0.016	174602	0.0624 ± 0.0002	696.69 ± 13.78

CRONUS-A measurements since October 2013. Values are consistent with a previosuly reported long-term CRONUS-A value of 655.17 ± 30.87 x 10^3 ^{14}C atoms g^{-1} (Young et al., 2014). We note, however, that beginning with the CRONUS-A-3-24-15 extraction, we started working with a new aliquot of the CRONUS-A quartz standard.

Table 4: Summary of deglacial radiocarbon ages

Location (Fig. 1)	Latitude	Longitude	^{14}C years	1-sigma uncertainty	cal yr BP	Setting (Site; Lab ID; material; desciption)	Reference
1	76	16	16750	110	19610 ± 170	JM02-460PC; AAR-8764; *N. pachyderma* ; Hemipelagic deposits above till	Rasmussen et al., 2007
2	76.4	13.1	19310	140	22660 ± 170	JM03-373PC2; AAR-8773; *N. pachyderma* ; Hemipelagic deposits above debris flow	Rasmussen et al., 2007
3	76.333	12.600	19630	150	23040 ± 230	JM03-374PC; AAR-8766; *N. pachyderma* ; Hemipelagic deposits above debris flow	Jessen et al., 2010
4	77.220	12.625	16880	80	19750 ± 170	NP90-46; Beta-71988; *E. excavatum* ; Marine sediment above diamicton	Cadman, 1996
5	77.617	9.936	16035	130	18780 ± 135	NP90-36; Tua-845; *N. pachyderma;* Above till, glaciomarine with IRD of Svalbard origin	Elverhøi et al., 1995
6	77.817	9.093	19815	120	23240 ± 190	NP90-39; Tua-557; *N.pachyderma* ; above till, glaciomarine with IRD of Svalbard origin	Elverhøi et al., 1995
7*	78.7588	10.7463	NA	NA	20290 ± 2120	JL00-31 Leefjellet; Beryllium-10 exposure age	Landvik et al., 2013
8*	79.2388	11.8139	NA	NA	25010 ± 1010	Langskipet; Beryllium-10 exposure age; 611 m a.s.l.	Gjermundsen et al., 2013
9*	79.4640	11.3937	NA	NA	21840 ± 950	Kaf-1; Beryllium-10 exposure age; 836 m a.s.l.	Gjermundsen et al., 2013
10*	79.6013	11.7866	NA	NA	19340 ± 1260	Average of Ovo-3 & Ovo-4; Beryllium-10 exposure ages; 687 m and 730 m a.s.l.	Gjermundsen et al., 2013
11*	79.7216	10.9483	NA	NA	17860 ± 2040	Average of 99-01 & 99-05 Danskøya; Beryllium-10 exposure ages; 77 m and 74 m a.s.l.	Landvik et al., 2003; Gjermundsen et al., 2013
12*	79.7375	13.6142	NA	NA	21670 ± 1310	R4; Beryllium-10 exposure age; 85 m a.s.l.	Gjermundsen et al., 2013
13*	80.2088	22.4817	NA	NA	26730 ± 3910	Bluffen-2; Beryllium-10 exposure age; 165 m a.s.l.	Hormes et al., 2011
14*	80.2073	22.5102	NA	NA	28270 ± 2140	Bluffen-3; Beryllium-10 exposure age; 123 m a.s.l.	Hormes et al., 2011
15	79.095	25.095	18640	100	21990 ± 170	GC06; NA; Bulk sediments; Mud above diamict	Hogan et al., 2010
16	76.7	16.4	10660	220	11730 ± 400	Werenskioldbreen; U-2831; *Mya truncata* (reworked); glacier margin near medial moraine	Birkenmajer and Olsson, 1998
17	77.08	15.18	10790	160	12100 ± 320	Werenskioldbreen; U-2972; *Mya truncata* (reworked); esker in glacier forefield	Birkenmajer and Olsson, 1998
18	77.55	14.03	12350	145	13690 ± 170	Wedel Jarlsberg/Dyrstadalen; Ua-1081; shell fragment; beach gravels at 50.5 m a.s.l.	Salvigsen and Elgersma, 1991
19	78.188	9.943	15255	180	17930 ± 230	NP90-21; Tua-359; *N. pachyderma;* Marine sediment above diamicton	Elverhøi et al., 1995
20	78.022	11.857	12835	100	14360 ± 250	NP-90-25; Tua-553; unidentified Mollusc; Glaciomarine mud over massive till	Svendsen et al., 1996
21	78.047	12.988	12985	145	14630 ± 330	88-02; Tua-42; *Nucula tenuis;* mud with dropstones on firm diamicton	Svendsen et al., 1992
22	78.071	13.759	12740	190	14260 ± 360	Linnevatnet; Ua-732, Shells; Marine sediment above diamicton	Mangerud and Svendsen, 1990
23	78.293	14.803	10975	60	12390 ± 150	JM98-818-PC; Tua-5191; Foraminifera; Glacimarine sediments on glaciomarine diamicton	Forwick and Vorren, 2009
24	78.277	15.260	10835	140	12180 ± 180	NP87-144; Ua-757; Mollusc unidentified	Elverhøi et al., 1995
25	78.380	15.479	11025	90	12430 ± 150	90-03 PC; Tua-442; Foraminifera; Laminated glacimarine mud on top of till	Elverhøi et al., 1995
26	78.565	16.428	10085	115	10980 ± 160	NP90-01-PC; Tua-186; Bryzoyoa; Marine mud on top of laminated deglaciated mud	Svendsen et al., 1996
27	78.552	16.540	10240	60	11130 ± 80	Kapp Ekholm V-H8; Ua-35635; *Hiatella arctica* ; Marine sands on LGM melt-out/subglacial till	Hormes et al., 2013
28*	78.8400	10.6023	NA	NA	16470 ± 1900	JL-00-10; Beryllium-10 exposure age; 325 m a.s.l.	Landvik et al., 2003
29	79.022	11.104	13960	120	16180 ± 190	NP90-9-PC3; WHG-941; Mixed benthic formas; Laminated marine mud over glacial till	Landvik et al., 2013
30*	79.1914	12.0009	NA	NA	16930 ± 1120	Flakstor; Beryllium-10 exposure age; 217 m a.s.l.	Gjermundsen et al., 2013
31*	79.7447	13.0695	NA	NA	15570 ± 790	R10; Beryllium-10 exposure age; 84 m a.s.l.	Gjermundsen et al., 2013
32*	80.0367	18.7056	NA	NA	16810 ± 1220	Flora-2; Beryllium-10 exposure age; 220 m a.s.l.	Hormes et al., 2011
33	80.355	16.299	14165	135	16470 ± 230	NP94-51SC2; mixed benthic foraminiferae; outer shelf	Koç et al., 2002

All radiocarbon ages were calibrated with Calib 7.1 and the MARINE13 database (Stuiver et al., 2017), and use a ΔR value of 107 ± 52 years (Mangerud et al., 2006; Hormes et al., 2013). Calibrated ages and their uncertainties have been rounded to the nearest decade. Note that locations marked with an asterisk report ^{10}Be ages and are reported as years of exposure, not years BP, and have been re-calcualted using the v3 of the CRONUS calculator (see main text).